Novel method for accurately estimating membrane transport properties and mass transfer coefficients in reverse osmosis

Yuanzhe Liang [a], Alexander V. Dudchenko [b], Meagan S. Mauter [a],[*]

[a] *Department of Civil & Environmental Engineering, Stanford University, Stanford, CA, 94305, USA*
[b] *Applied Energy Division, SLAC National Accelerator Laboratory, Menlo Park, CA, 94025, USA*

ABSTRACT

We present a simple and robust method to simultaneously characterize the water and salt permeability (*A, B*) of reverse osmosis (RO) membranes and mass transfer coefficient (*k*) in membrane modules. The proposed methodology comprises a set of RO experiments performed at different operating pressures or stages. The measured water and salt fluxes in each stage are simultaneously fitted to the RO transport equations by performing a nonlinear regression, using *A*, *B*, and *k* as regression parameters. We first perform a systematic accuracy analysis of the proposed method across the full operational range of RO. The assessment shows that the method accuracy is substantially higher than current methods and increases with number of experimental stages and driving forces. This assessment is used to inform the design of an experimental protocol that minimizes errors in estimated *A*, *B*, and *k*. We then evaluate two commercial RO membranes following the new protocol. For both membranes, *A* and *B* parameters decrease by 17% and 15% from the dilute solution to seawater concentrations, whereas the *k* parameter remains constant. Our study demonstrates that the proposed method, informed by data-driven experimental designs, provides a new approach for accurately characterizing transport phenomenon in membrane processes with feeds of less than 100 g/L total dissolved solids.

1. Introduction

Membrane-based desalination processes represent an efficient and sustainable separation technology platform for water purification [1–7]. Seawater reverse osmosis (SWRO) desalination (feed ~35 g L⁻¹; π ~ 28 bar) remains the most energy-efficient and cost-effective separation process for freshwater production from seawater [8,9]. Extensions of the RO process to hypersaline brines (feed up to 250 g L⁻¹; π up to 300 bar) may also enable zero liquid discharge (ZLD) [10–12].

Central to these technologies is a semipermeable membrane capable of separating pure water from seawater or brine [3,13–15]. The performance of the RO membrane is generally described using the water permeability coefficient (*A*) and salt permeability coefficient (*B*) [16]. However, the measurement of *A* and *B* values in RO has always been complicated by the formation of a concentration polarization (CP) layer, which leads to a higher osmotic pressure at membrane-water interfaces [17–19]. This osmotic pressure must be accurately established in order to determine the net driving force and calculate *A*, and *B* [20].

Standard methods for measuring RO membrane parameters are designed for measurements at low salt concentrations that minimize the formation of CP or attempt to approximate it empirically [21]. The most common method involves two separate experiments [22]. In the first experiment, the water permeability is measured using deionized water as feed, where no CP forms and driving force is proportional to applied hydraulic pressure. This allows for direct calculation of the *A* parameter. Under the assumption that *A* does not change in the presence of salt, a second experiment is performed using the same membrane and a feed concentration of 100–1000 ppm (seawater TDS is ~35,000 ppm) [22]. Assuming that the CP is negligible under these low bulk TDS conditions, the *B* parameter can be estimated by comparing the bulk salt concentrations in the feed and permeate streams. Although this method is valid for measuring *A* and *B* in low salinity conditions, it does not allow direct measurement of *A* and *B* in high salinity conditions, where the polyamide layer is expected to dehydrate and its transport properties to change.

The other most commonly used method overcomes this problem by characterizing *A* and *B* parameters simultaneously from the estimates of the driving force [23,24]. Specifically, surface concentration in the boundary layer is first calculated based on film theory to account for the CP [17]. Next, *A* is determined by dividing the water flux by the osmotic
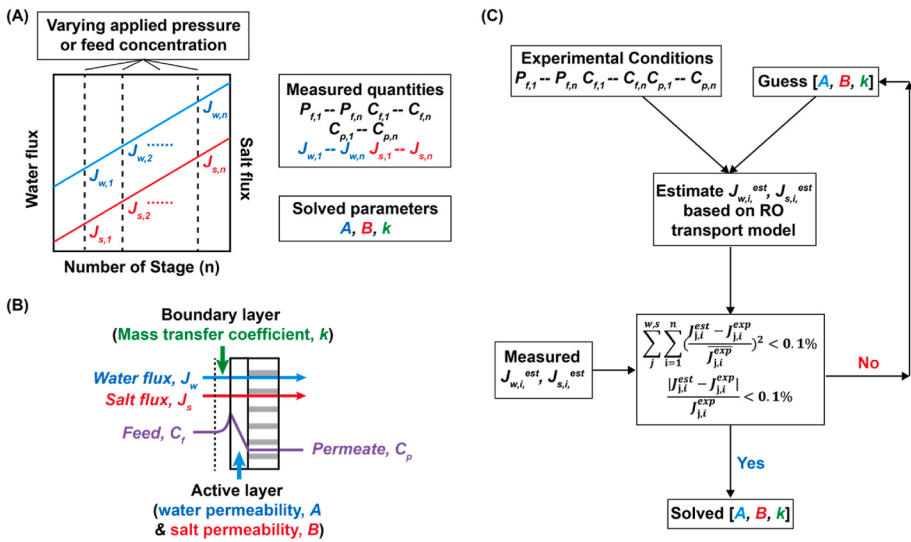
Fig. 1. Protocol of the proposed method. (A) A single RO experiment is conducted over several stages (N ≥ 2) with varying applied pressure or feed concentrations. Measured quantities including pressure, $P_{f,n}$, feed concentration, $C_{f,n}$, permeate concentration, $C_{p,n}$, water flux, $J_{w,n}$, and salt flux, $J_{s,n}$, at each stage are simultaneously used to solve for membrane parameters, A and B, mass transfer coefficient, k. (B) Schematic of water flux, salt flux, and salt concentration profile across a RO membrane. (C) Flowchart for the calculation of A, B, and k parameters using the proposed RO method.

pressure difference across the membrane and B is determined by dividing the salt flux by the concentration gradient across the active layer. Both calculations rely on accurate estimation of the mass transfer coefficient in the boundary layer, the accuracy of which varies significantly depending on the validity of empirical correlations over the cell dimensions and flow regimes used in the experimental setup [25].

Accurately estimating mass transfer rates is also critical for validating CP layer theories. Standard CP theory assumes a stagnant thin film model with one-dimensional flow and a fully developed boundary layer in which mass transfer occurs across a stagnant film of thickness δ (function of module length) [26]. This model ignores the impact of permeate convection on the film layer thickness, and its validity for multi-component salts is not known. Recently, more complex empirical models have been developed, e.g., retained solute (RS) model [27,28] and numerical convection–diffusion (CD) model [17], to include the impact of locally varying permeate flux on the development of boundary layer. Both the standard and modified CP models rely on empirical Sherwood correlations to estimate mass transport rates that, as described above, are prone to misapplication [22].

Directly quantifying the mass transfer coefficient is challenging due to the uncertainty of empirical methods and the lack of clear guidance on the respective accuracy of each approach. The standard method of calculating the k parameter involves first estimating the Sherwood number (Sh) using either the laminar or turbulent flow correlation for a rectangular channel and then calculating k using the film model [29]. Similar empirical methods were developed for measuring k and level of CP based on film theory. For example, Sutzkover et al. proposed a technique to determine k by measuring the flux decline induced by the addition of a salt solution to an initially salt-free water feed [30]. Alternatively, Mahmood et al. reported an indirect method to estimate the mass transfer coefficient based on the measurement of dissolution of a plate of benzoic acid in water [23]. The benzoic acid concentration in the water was measured by UV–vis as a function of time, allowing the calculation of the mass transfer coefficient [23]. However, the accuracy of these methods has never been fully quantified.

As alluded to below, uncertainty in the accuracy of the methods or imprecision in experimental measurements can lead to large errors in the estimated parameters. Our recent work carried out a systematic accuracy analysis of all existing methods for characterizing membrane parameters in RO/HPRO, forward osmosis (FO), pressure retarded osmosis (PRO), and osmotically assisted reverse osmosis (OARO) [21]. The result demonstrated that the direct RO method was extremely prone to random errors in measured quantities. For instance, a small random error (up to ± 1%) in measurement can induce a median error of 22%

and a 95th error of 182% in the estimates of water permeability using the direct RO calculation method. Whereas the inclusion of multistage measurements and optimization of experimental conditions can significantly reduce both methodological and measurement errors. Therefore, a smart design of experimental protocol based on data-driven analysis is critical to minimizing methodological errors and measurement errors.

In this work, we present a novel method for characterizing membrane transport properties and mass transport coefficients in the boundary layer using a single RO experiment. This protocol consists of a RO experiment divided into multiple stages by varying applied hydraulic pressure. All measured water and salt fluxes are simultaneously fitted to the RO transport equations, using A, B, and k as the regression parameters. To demonstrate the generalizability of this protocol, we perform a systematic analysis of the accuracy and robustness of the proposed method. This assessment also allows us to identify a set of ideal experimental conditions that minimize errors in A, B, and k.
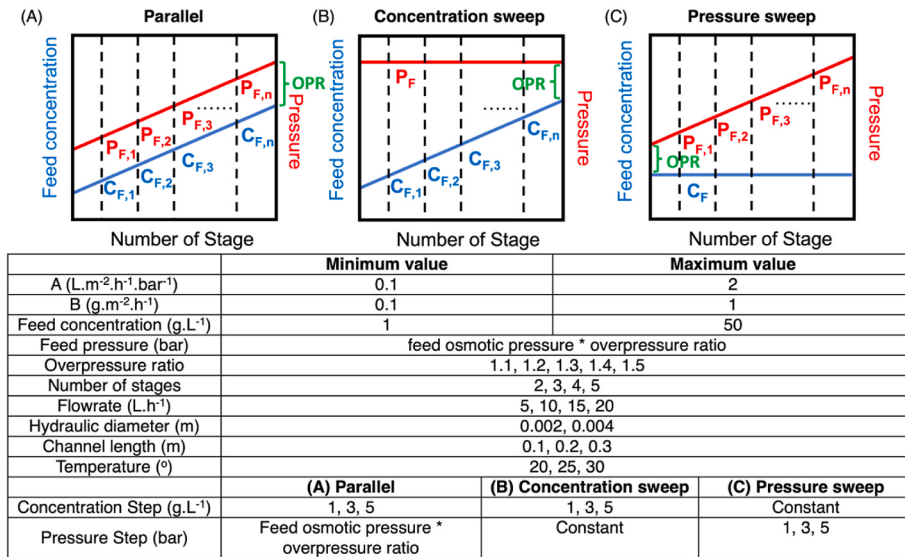
Following this protocol, we characterize A, B, and k parameters of two commercial RO membranes (i.e., SW30 and BW30) as a function of salinity and crossflow rate. The results of our study confirm that water and salt permeabilities of TFC-RO membranes decrease with increasing salinity and that the mass transfer coefficient in the boundary layer increases with increasing crossflow velocity. Finally, we discuss challenges associated with characterizing the effect of high salinity (>100 g/L TDS) on transport parameters using current membrane characterizing protocols and identify critical needs in the further development of direct or empirical methods with higher accuracy for quantifying the high-salinity effect on membrane transport properties.

2. Materials and methods

2.1. Proposed protocol for characterizing membrane parameters and mass transfer coefficient in the boundary layer in a single RO experiment

We propose a single RO experiment to characterize the intrinsic transport parameters, A and B of an RO membrane, and the mass transfer coefficient k in the boundary layer by measuring the water and salt flux across the membrane under varying applied pressure or feed concentrations (Fig. 1A). The design matrices of the RO experiment include the number of stages (N ≥ 2), overpressure ratio, pressure increment by stage, feed concentration increment per stage, temperature, crossflow rate, and filtration cell dimensions. The influence of each design parameter will be discussed in Section 2.3.

We developed a data-driven computational approach for optimizing the experimental protocol to maximize the accuracy and robustness of A,

Fig. 2. Parameter ranges used for process data set generation in three experimental design protocols. (A) Parallel increases in feed concentration and pressure. The feed concentration increases by a certain step size (e.g., 1 or 3 or 5 g/L) per stage, and the applied pressure is increased by multiplying the current feed osmotic pressure by a fixed overpressure ratio (OPR). (B) Concentration sweep. The feed concentration increases by a certain step size per stage while maintaining a constant pressure equal to the final feed osmotic pressure times the overpressure ratio. (C) Pressure sweep. The feed concentration is constant throughout the RO experiment, while the applied pressure increases by a certain step size (e.g., 1, 3, or 5 bar). The initially applied pressure equals the feed osmotic pressure times the overpressure ratio.

	Minimum value		Maximum value	
A (L.m⁻².h⁻¹.bar⁻¹)	0.1		2	
B (g.m⁻².h⁻¹)	0.1		1	
Feed concentration (g.L⁻¹)	1		50	
Feed pressure (bar)	feed osmotic pressure * overpressure ratio			
Overpressure ratio	1.1, 1.2, 1.3, 1.4, 1.5			
Number of stages	2, 3, 4, 5			
Flowrate (L.h⁻¹)	5, 10, 15, 20			
Hydraulic diameter (m)	0.002, 0.004			
Channel length (m)	0.1, 0.2, 0.3			
Temperature (°)	20, 25, 30			
	(A) Parallel	**(B) Concentration sweep**	**(C) Pressure sweep**	
Concentration Step (g.L⁻¹)	1, 3, 5	1, 3, 5	Constant	
Pressure Step (bar)	Feed osmotic pressure * overpressure ratio	Constant	1, 3, 5	

A (L.m^{-2}.h^{-1}.bar^{-1}); B (g.m^{-2}.h^{-1}); Feed concentration (g.L^{-1}); Flowrate (L.h^{-1}); Concentration Step (g.L^{-1})

B, and k parameter measurements. The ideal RO experiment consisted of five stages. We maintained a constant feed concentration in all five stages while increasing the applied pressure by a constant value per stage. The increase in the driving force led to an increase in water flux and salt flux at each stage, allowing us to measure the five sets of water and salt fluxes in the single RO experiment.

2.2. Determining the membrane transport properties and the mass transfer coefficient in the boundary layer

2.2.1. Water and salt flux governing equation in RO

The governing equation of water and salt flux in RO can be derived from the mass transport across the RO membrane. A schematic of the salt concentration profile across a RO membrane is shown in Fig. 1B. The water flux, J_w, and salt flux, J_s across the active layer are given by Ref. [31]:

$$J_w = A\left(P_f - \left(\pi_{f,m} - \pi_p\right)\right) \tag{1}$$

$$J_s = B\left(C_{f,m} - C_p\right) \tag{2}$$

Where A is the water permeability, B is the salt permeability, P_f is the feed pressure, $\pi_{f,m}$ is the osmotic pressure at the membrane surface, π_p is the osmotic pressure of the permeate, $C_{f,m}$ is the salt concentration at the membrane surface, C_p is the salt concentration of the permeate.

Due to the selective passage of water across the RO membrane, rejected salt accumulates at the membrane surface. This results in a localized concentration gradient in the boundary layer defined as external concentration polarization (ECP). At steady state, the salt flux across the active layer is equal to the salt flux in the boundary layer [31]:

$$J_s = -D_s \frac{dC}{dx} + J_w C \tag{3}$$

Where D_s is the diffusion coefficient of salt in the boundary layer, and C is the salt concentration at the distance of x relative to the membrane.

Integrating Eqn. (3) across the boundary layer thickness, from the bulk solution ($x = 0$, $C = C_f$) to the surface of membrane ($x = \delta$, $C = C_{f,m}$), yields:

$$C_{f,m} = C_f \exp\left(\frac{J_w}{k}\right) + \frac{J_s}{J_w}\left(1 - \exp\left(\frac{J_w}{k}\right)\right) \tag{4}$$

Where $C_{f,m}$ is the salt concentration at the feed-membrane interface, C_p is the salt concentration in the permeate, and $k = \frac{D}{\delta}$ is the boundary layer mass transfer coefficient.

Based on Eqn. (4), the water and salt flux in Eqns. (1) and (2) can be expressed in terms of membrane parameters, A and B, mass transfer coefficient in the boundary layer, k, and experimentally accessible parameters, P_f, C_f, C_p, J_w, J_s.

2.2.2. Calculating A, B, and k numerically by minimizing global error
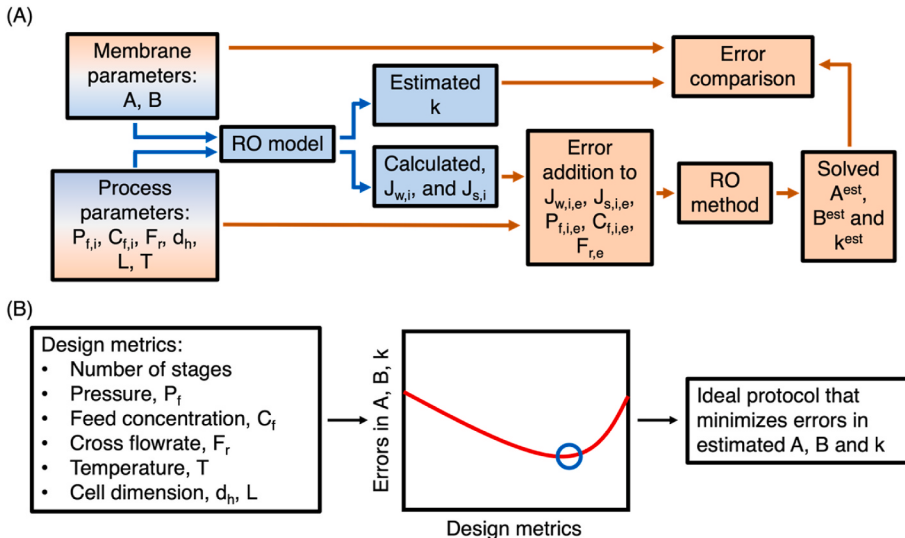
We utilize a differential evolution algorithm to minimize the maximum likelihood objective function to calculate membrane parameters, A and B, and mass transfer coefficient, k, from the experimentally measured water and salt flux data. By following the five-stage procedure outlined in Section 2.1, ten values of water flux and salt flux were collected during a single RO experiment, i.e., $J_{w,i}^{exp}$ and $J_{s,i}^{exp}$, where $i = 1$, 2, 3, 4, 5 denotes the stage of the experiment. In addition, we also recorded the feed concentration (C_f), temperature (T), permeate concentration ($C_{p,i}$, where $i = 1, 2, 3, 4, 5$), applied pressure ($P_{f,i}$, where $i = 1, 2, 3, 4, 5$). We used the standard differential evolution solver in Scipy to fit a group of five experiment conditions to Eqns. (1), (2) and (4), using A, B, and k as regression parameters [32]. We set the bound for A as [1e-3, 50], bound for B as [1e-4, 50], bound for k as [1e-6, 1], respectively. The ten transport equations and three unknowns (A, B, and k) constitute an over-determined system of non-linear equations, amendable for the numerical solution by minimizing the global error in the estimated fluxes and measured values. The global error, E, is defined as the non-dimensional sum of the difference between estimated and experimentally measured water and salt fluxes using the maximum likelihood objective function formulation [33,34]:

$$E = E_w + E_s = \sum_{i=1}^{n_{exp}} \left(\frac{J_{w,i}^{est} - J_{w,i}^{exp}}{\sigma_{J_{w,i}}^{exp}}\right)^2 + \sum_{i=1}^{n_{exp}} \left(\frac{J_{s,i}^{est} - J_{s,i}^{exp}}{\sigma_{J_{s,i}}^{exp}}\right)^2 \tag{5}$$

Where n is the number of stages and is equal to 5 in this study, $\sigma_{J_{w,i}}$ is the standard deviation of water flux at each stage, and $\sigma_{J_{s,i}}$ is the standard deviation of salt flux at each stage.

The goodness of the fit was checked by computing the absolute difference between estimated fluxes and experimentally measured fluxes in Eqn. (6). We proved that Eqn. (6) is a more stringent quality control than the coefficient of determination [22] in the Supplementary section A.

$$Err_{abs,w,i} = \frac{\left|J_{w,i}^{est} - J_{w,i}^{exp}\right|}{J_{w,i}^{exp}} \leq 0.1\% \tag{6}$$

Fig. 3. Proposed framework for (A) process simulation and error analysis, (B) search for ideal experimental protocol. The process data for RO is simulated using the solution-diffusion model that balances the mass transfer across the membrane. The inputs including membrane and process parameters are sampled across a bounded range using a Monte Carlo approach. The output water, salt flux, and the original process parameters with no error, or random errors with/without biased errors added in one or more process parameters, are used to calculate membrane parameters using the proposed method. The error is assessed by comparing the difference between the original membrane parameter inputs and the predicted membrane parameters. The ideal experimental protocol is generated by scanning through all design metrics to minimize the effect of random and biased errors on the accuracy of the proposed method.

2.2.3. Assumptions of the proposed method

We assume that the membrane reflection coefficient approaches unity (i.e., $g = 1$). Therefore, the proposed method is only valid for tight, salt-rejecting membranes that can maintain virtually the entire osmotic pressure difference across its active layer [35].

We assume that the membrane transport properties, A and B, and mass transfer coefficient, k, are independent of the change of pressure within each RO experiment. To minimize the effect of pressure on A and B [36], we carried out the RO experiment using a small pressure step of 10 psi per stage and a total pressure sweep of 40 psi in the entire experiment. Similarly, we neglect the effect of pressure on the level of ECP (i.e., k) within each RO experiment. All solution physical properties are dependent on the salinity and temperature [37,38].

In the theoretical validation of the proposed method, we assume that the random measurement errors are independent and identically distributed (IID) random variables [34].

The use of our proposed method for membrane parameter estimation is only valid when the measurement errors are small, such that that uncertainties in the independent variables are negligible compared to uncertainties in the dependent variables of the nonlinear model [33,39]. Therefore, we recommend that users follow measurement guidelines detailed in our previous work to minimize the random errors in the measured parameters [21].

2.3. Theoretical validation of the proposed method

We first performed a systematic analysis to evaluate the accuracy and robustness of the proposed method for determining A, B, and k parameters. In the analysis, we simulate the RO process using a standard mass balance model. We assess the effect of methodological error, random measurement error, and biased measurement errors on the accuracy of estimated A, B, and k parameters. The result of this analysis further guides the data-driven design of experimental protocol with high accuracy and robustness.

2.3.1. Generation of process data

We generated three sets of RO data in three experimental designs (Fig. 2), (1) parallel increase in pressure and salinity, (2) concentration sweep with constant pressure, and (3) pressure sweep with a constant salinity. We simulated the full range of RO operating conditions via a random selection of process parameters and membrane parameters from a uniform distribution using the Monte Carlo approach (Fig. 2). The range of membrane parameters represents the typical values reported in the literature [40]. The model input parameters consisted of membrane

parameters, module design parameters, and operating conditions, while the output data included the mass transfer coefficient, water flux, and salt flux (Fig. 3A). The mass transfer coefficient was calculated from the Sherwood number [29,41]:

$$Sh = 1.85 \left(ReSc \frac{d_h}{L} \right)^{0.33} \tag{7}$$

$$Sh = 0.04 Re^{0.75} Sc^{0.33} \tag{8}$$

where Re is the Reynolds number, Sc is the Schmidt number, d_h is the hydraulic diameter, and L is the length of the channel. By using the tabulated diffusion coefficient, D, data from Lobo et al. [42], the mass transfer coefficient, k, can be calculated from:

$$Sh = kd_h/D \tag{9}$$

We generated 50,000 data sets for each experimental design. Our selected solver was able to solve ~99% of randomly generated combinations of input parameters, terminating when the change in water and salt flux was <0.1%. The CDFs of input parameters and output data are shown in Supplementary section B (Supplementary Figs. S1–3).

2.3.2. Error addition to process data

We first evaluated the accuracy of the proposed method without accounting for experimental error in the three proposed protocols (1) parallel, (2) concentration sweep, and (3) pressure sweep. Next, we assessed the effect of random errors and biased errors in measured data on the accuracy of the three proposed methods (Fig. 3A). A random error (up to ± 0.5%) was added to at least one process parameter including feed and permeate concentration, water and salt flux, pressure, temperature, and flow rate. A biased error (up to + 5%) was added to pressure. All errors were randomly generated from a uniform distribution and were introduced to the parameters prior to analysis. We analyzed each data set ten times with different errors, expanding the size of the testing data set from 50,000 to 500,000.

2.3.3. Analysis of accuracy of the proposed methodology

We analyzed the accuracy of the proposed method (Eqn. (10)) by comparing the estimated A, B, and k solved by the method with the input A and B, and k calculated using Eqns. (7)–(9):

$$Err_{abs,X} = \frac{\left| X^{est} - X^{input} \right|}{X^{input}} \times 100\% \tag{10}$$

Here, X^{est} is the estimated membrane parameters and mass transfer

coefficient. We reported the median error and 95th percentile error of estimates. The median error represents the middle value of the errors in all estimated membrane parameters, and the 95th percentile represents the value that is greater than 95% of all errors.

We compared the performance of the proposed method in three experimental designs, (A) parallel, (B) concentration sweep, and (C) pressure sweep, to identify the ideal experimental protocol with high accuracy and robustness. We also evaluated the effect of individual design metrics on accuracy of the proposed method.

2.3.4. Validation of mass transfer coefficient

We validated the estimated mass transfer coefficient in the boundary layer in the RO system using an empirical method [30]. This method was based on the evaluation of the permeate decline induced by the addition of salt to an originally salt-free water feed. The decline of permeate flux due to the osmotic pressure prevailing at the membrane surface enables the estimation of salt concentration at the membrane surface, and hence the determination of mass transfer coefficient k. The mass transfer coefficient is calculated by:

$$k = \frac{J_{w,salt}}{\ln\left(\frac{\Delta P}{\pi_{feed} - \pi_{permeate}}\left(1 - \frac{J_{w,salt}}{J_{w,salt-free}}\right)\right)} \quad (11)$$

Where $J_{w,salt-free}$ and $J_{w,salt}$ are the measured permeate fluxes before and after the addition of salt to the pure water feed, respectively, ΔP is the applied pressure, π_{feed} and $\pi_{permeate}$ are the osmotic pressure of the feed and the permeate after salt addition.

2.4. Implementation of the proposed method

2.4.1. Materials

We characterized two commercial thin-film-composite reverse osmosis membranes, BW30 and SW30-XLE, (Dow Chemical Company, Midland, MI). Three separate samples for each membrane type were employed. NaCl (>99%) was purchased from Fisher Scientific (US). Deionized water (Millipore, US) was used for solution preparation and membrane cleaning.

2.4.2. Experimental procedure

We characterized the water and salt flux of RO membranes in a crossflow RO system (Sterlitech, CF042). The cell has an effective membrane area of 42 cm². A Danfoss App.06 pump was used to circulate the salt solution in closed loops at a crossflow velocity of between 0.557 cm/s and 1.11 cm/s. A chiller held the temperature of the feed solution at 20 ± 0.1 °C. The feed concentration was automatically maintained at a fixed value by using a feedback control scheme that measured feed conductivity and added permeate from the RO to the feed tank when the conductivity increased above the set point. This allowed us to control the conductivity within ~0.1% of the set value.

All membranes were pre-compacted in DI water at 600 psi for 24 h prior to measurement to ensure that the pure water flux remained stable over the experimental pressure range. At the beginning of the first measurement, an appropriate volume of the NaCl stock solution was added to the feed tank to obtain the desired concentration and initiate the first stage. All experimental parameters including pressure, temperature, conductivity of feed, conductivity of permeate, and weight of the permeate, were logged throughout the RO experiment. Concentrations were determined with a calibrated conductivity meter (Oakton Instruments, Vernon Hills, IL). Water flux was determined by monitoring the rate of change in weight of the permeate. Salt flux at steady state was calculated using ($J_s = J_w * C_p$). Although the water flux and permeate concentration stabilized quickly, we kept it running for 4 h in the first stage. The second stage began by increasing the applied pressure by 10 psi and data logging continued for 2 h. The procedure was repeated for the third, fourth, and fifth stages (Supplementary Fig. S4).

We characterized the effect of crossflow velocity and salinity on

Table 1
Complete set of RO experimental conditions.

Membrane type	Pressure (psi)	Feed (g. L⁻¹)	Crossflow velocity (cm. s⁻¹)
BW 30	600, 610, 620, 630, 640	1	0.557
			0.892
			1.11
SW 30		10	1.11
		20	1.11
		30	1.11
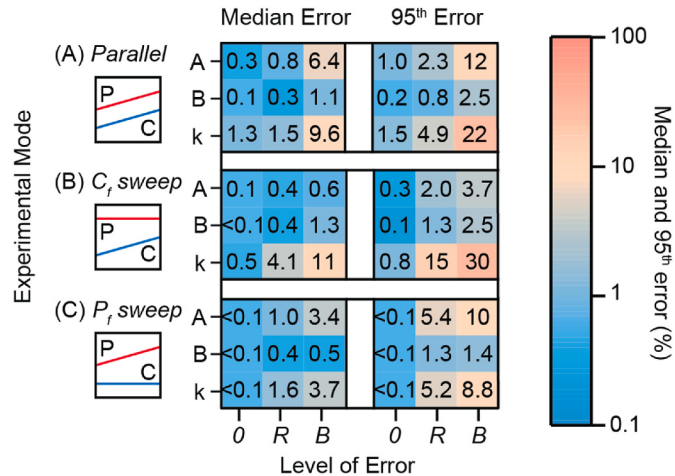
Fig. 4. Heatmap of the median error and 95th percentile error of estimated *A, B,* and *k* parameters using the proposed 5-stage method in three experimental modes (A) Parallel increase in concentration and pressure, (B) Concentration sweep with a constant overpressure, (C) Pressure sweep with a constant feed concentration. Red solid line in the schematic indicates the pressure profile, and blue solid line indicates the feed concentration profile. The X-axis of the heatmap denotes the type of error added to the input parameter. 0 represents no errors added, R represents a random error up to ±0.5% added to all input parameters, and B represents a biased error up to +5% added to the feed pressure in addition to random errors. Y-axis of the heatmap denotes the parameters estimated by the method. The median error represents the value in the middle of all errors, and the 95th percentile represents the value that is greater than 95% of all errors. The blue colors indicate a small error and red colors indicate a large error in estimates, respectively. The process parameters used for RO data generation and error analysis in the figure are: concentration range from 0 to 50 g/L, overpressure ratio of 1.5, flowrate of 5 L/h, hydraulic diameter of 0.002 m, channel length of 0.3 m, concentration step of 1 g/L in (A) and (B), and pressure step of 1 bar in (C). (For interpretation of the references to color in this figure legend, the reader is referred to the Web version of this article.)

transport parameters, *A* and *B* of the RO membrane, and mass transfer coefficient, *k*, in the boundary layer. The experimental conditions were summarized in Table 1.

3. Results and discussion

Accurately measuring the membrane transport parameters and mass transfer coefficient is challenging due to the uncertainty in empirical methods that rely on simplified assumptions and imprecision in experimental measurements. In this work, we proposed a data-driven design protocol for simultaneous characterization of membrane parameters, *A* and *B*, and mass transfer coefficient, *k*, with high precision.

We began by performing a systematic accuracy analysis to validate the robustness and reliability of the proposed methodology in three different experimental designs. Next, we scanned through the design matrix of the operating parameters, including the number of stages, overpressure ratio, increment of pressure per step, crossflow velocity, and cell dimensions, to identify the experimental protocol with the
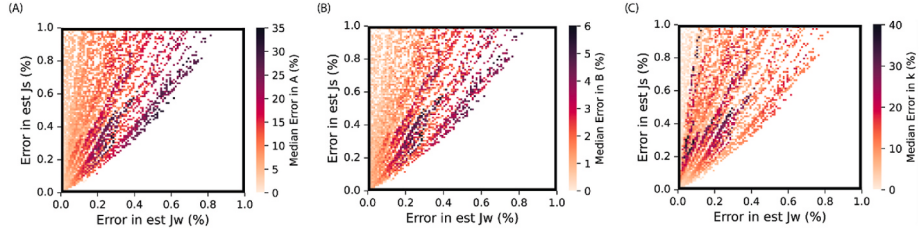
Fig. 5. Median error in the estimates of (A) water permeability, (B) salt permeability, and (C) mass transfer coefficient as a function of the absolute error in water flux and salt flux. The simulated result is generated using the pressure method in the pressure-sweep mode. The condition for the data simulation is outlined in Fig. 2.

highest accuracy. Following this protocol, we measured the membrane transport parameters, A and B, of two commercial TFC-PA RO membranes, i.e., SW30 and BW30, and mass transfer coefficient, k, in the boundary layer, as a function of feed salinity and crossflow velocity.

3.1. Robustness and reliability of the methodology

3.1.1. Accuracy of the proposed method in three RO experimental modes

We analyzed the accuracy of the proposed method for estimating membrane parameters, A and B, and mass transfer coefficient, k, using three distinct RO experimental modes. In the parallel mode (Fig. 2A), we

simultaneously increase the feed concentration and the applied pressure per stage. The applied pressure is calculated by multiplying the feed osmotic pressure at each stage with a constant overpressure ratio. In concentration sweep (Fig. 2B), we increase the feed concentration per stage while maintaining the constant pressure that is equal to the final feed osmotic pressure times the overpressure ratio. In pressure sweep (Fig. 2C), we maintain a constant feed concentration throughout the RO experiment while increasing the applied pressure per stage.

The parallel and concentration sweep modes are susceptible to impact of random errors and biased errors, resulting in poor estimates of the k parameter. In the parallel mode (Fig. 4A), the 95th error in
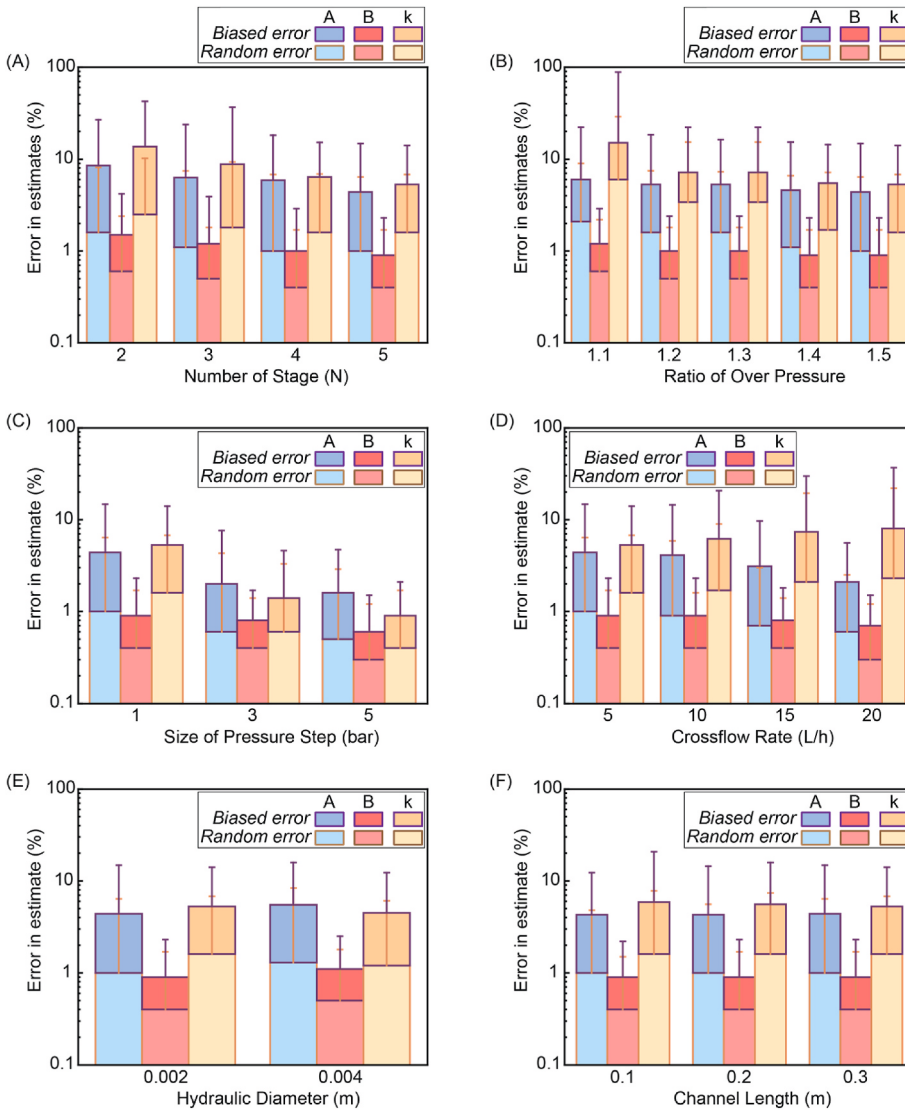
Fig. 6. Effect of individual parameters in the design metrics on the accuracy of proposed method using the pressure-sweep experimental protocol. (A) number of stages, (B) ratio of overpressure, (C) pressure step, (D) crossflow rate, (E) hydraulic diameter, and (F) channel length. The bottom three columns in light blue, light red, and light yellow indicate the median error in A, B, and k with the addition of random errors, and the corresponding error bar represents the 95th percentile error. The upper three columns in dark blue, dark red, and dark yellow indicate the median error in A, B, and k with the addition of random errors and biased error in pressure, and the corresponding error bar represents the 95th percentile error. (For interpretation of the references to color in this figure legend, the reader is referred to the Web version of this article.)

estimated k parameter increases to 4.9% with the addition of random errors and 22% with the addition of biased errors. In addition, using a constant pressure led to an even higher uncertainty in k parameter. The 95th errors in estimated k parameter increase to 15% with the addition of random errors and 30% with the addition of biased errors in the concentration-sweep mode (Fig. 4B). As random and biased errors are common in experiments, we do not advise using these two approaches.

The pressure-sweep mode in the proposed method shows the best overall performance due to its higher tolerance to random and biased errors. It also benefits from easier process operation. Although varying applied pressure increases the uncertainty of estimated A, using a constant feed concentration mediates the effect of biased error in pressure on the estimates of A. The median and the 95th percentile error in A remain as low as 3.4% and 10% with the addition of random and biased errors in pressure-sweep mode (Fig. 4C). More importantly, using a constant feed concentration significantly increases the accuracy of estimated k which remained at 0.1% without any errors in measurements, and the 95th percentile error remained below 5.2% and 8.8% with addition of random and biased errors, respectively. Finally, in a continuous multi-stage RO experiment, increasing the applied pressure can be swiftly performed by changing the controller setpoint in an automated system or manually adjusting the pressure regulator in a manual system.

3.1.2. Reliability of the methodology

Estimation methods require quantitative guidance on the accuracy of estimated parameters as a function of error in the fitted values. In this method, the accuracy of estimates in A, B, and k increase with a decrease in absolute error between measured and estimated water and salt flux values (Fig. 5). The normalized errors in the estimated parameters all converge towards zero as absolute errors between measured and estimated water and salt flux approach zero. In our simulated results for the five-stage pressure-sweep RO method, an absolute error in measured and estimated water flux and salt flux of less than 0.1% will yield a median error of 3.7% and a 95th error of 10% in the calculated parameters (Fig. 5).

3.2. Data-driven design of a high accuracy experimental protocol

We proposed a multi-stage characterization method based on a nonlinear regression of an over-determined system of equations to predict A, B, and k parameters in RO. The determination of three unknowns requires at least a 2-stage RO experiment with two pairs of measured water fluxes and salt fluxes. Other important design metrics include the overpressure ratio, size of the pressure step, crossflow rate, and flow cell dimensions. To identify an optimal experimental protocol that maximizes the accuracy and robustness of the membrane parameters measurements, we performed a systematic investigation of the effect of individual design parameters on the accuracy of the proposed method.
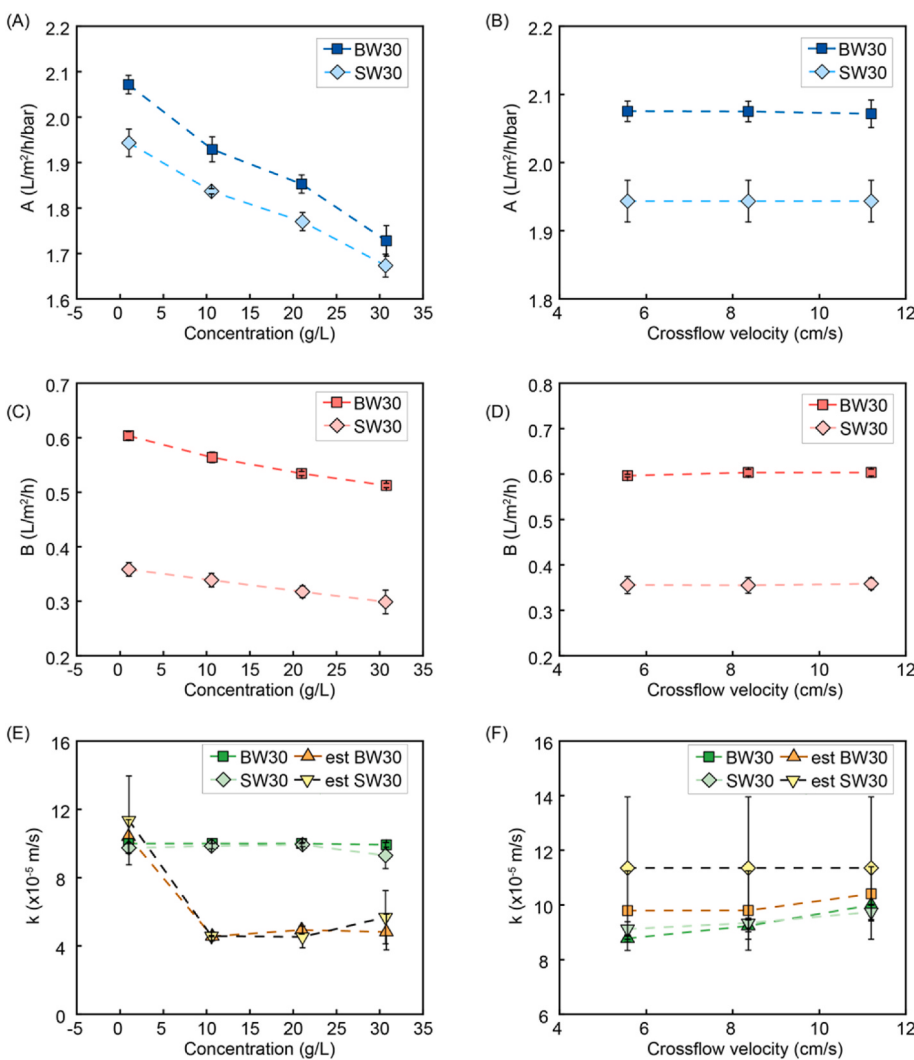
Fig. 7. Experimental measurement of (A, B) water permeability, A, and (C, D) salt permeability, B, of two commercial RO membranes, BW30 and SW30, as a function of feed salinity and crossflow velocity. (E, F) Experimental measurement of mass transfer coefficient, k, and estimation of k using reference method [30] in the boundary layer as a function of feed concentration and crossflow velocity. A single RO experiment comprised a 5-stage pressure sweep from 600 psi to 640 psi with a pressure increment of 10 psi per step.

3.2.1. Influence of the number of stages

Characterizing the membrane over a greater number of stages increases the accuracy of all three predicted parameters (Fig. 6A) because inevitable experimental errors are averaged out by a larger dataset. Specifically, the median error and 95th error in predicted *A* decrease from 6.9% to 18% in the 2-stage RO experiment to 3.4% and 10% in the 5-stage RO experiment, respectively. Similarly, the median error and 95th error in predicted *k* decrease from 11% to 29% in the 2-stage RO experiment to 3.7% and 8.8% in the 5-stage RO experiment, respectively.

3.2.2. Influence of the ratio of overpressure

Increasing the ratio of overpressure enhances the accuracy of all predicted parameters (Fig. 6B) because it minimizes the effect of measurement errors in concentration on the estimates of the driving force. At low-pressure conditions where the osmotic pressure of the feed is comparable to the applied pressure, the estimation of surface concentration and driving forces are sensitive to the changes in both bulk concentration and applied pressure. The influence of errors in concentration becomes minimal under high-pressure conditions because the applied pressure dominates the effective driving force. For example, the median error and 95th error in *k* decrease from 9.1% to 74%–3.7% and 8.8% as the ratio of overpressure increases from 1.1 to 1.5.

3.2.3. Influence of the size of pressure step

Increasing the size of pressure step also enhances the accuracy of the proposed method. For instance, the median error and 95th percentile error in *A* decrease from 3.4% to 10%–1.1% and 3.1%, and the median error and 95th percentile error in *k* decrease from 3.7% to 8.8%–0.5% and 1.2% when the step size of pressure increment increases from 1 bar to 5 bar. However, this analysis assumes that the effect of compaction during the 5-stage experiment on the membrane transport properties is negligible. Therefore, we suggest using a small step size of pressure to ensure a confident prediction of parameters using the proposed method.

3.2.4. Influence of the crossflow rate

While increasing the crossflow rate would increase the accuracy of estimated *A* and *B*, the accuracy of estimated *k* parameter is compromised (Fig. 6D). The median and 95th errors in *A* decrease from 3.4% to 10%–1.5% and 3.5%, but the median error and 95th error in *k* increase from 3.7% to 8.8%–5.7% and 29%. Increasing crossflow rate reduces the effect of CP in the boundary layer and increases the effective driving force. Consequently, the effect of random errors on estimated *A* and *B* decrease. However, the uncertainty in estimated *k* increases when the concentration gradient in the boundary layer decreases at a high crossflow rate. These results suggest a trade-off between accurately characterizing membrane transport properties and accurately characterizing the mass transfer coefficient in the boundary layer. In addition, it provides two avenues for characterizing transport phenomena in RO. One is to use a high crossflow rate to maximize the accuracy of estimated membrane transport parameters. The other is to use a low crossflow rate in order to better characterize the mass transfer coefficient in the boundary layer.

3.2.5. Influence of the flow cell dimension

The effect of crossflow rate on the accuracy of the proposed method applies to the design of flow cells (Fig. 6E and F). If one wants to characterize the membrane transport properties, a flow cell with a smaller hydraulic diameter and a smaller channel length should be used to maximize the accuracy of estimated *A* and *B*. In contrast, a more accurate characterization of the mass transfer coefficient should be performed using a flow cell with a bigger hydraulic diameter and channel length. Although changing flow rates is always easier than altering the dimension of flow cells, our analysis provides an important toolkit for quantifying the accuracy of each parameter using a specific flow cell.

3.3. Implementation of the proposed methodology

The above analysis informed the design of an optimal experimental protocol with high accuracy and robustness. Following this protocol, we characterized the membrane transport properties of two commercial TFC-PA RO membranes, BW30 and SW30, and the mass transfer coefficient of the boundary layer in RO. A detailed experimental procedure is outlined in Section 2.4.

3.3.1. Effect of salinity on A, B, and k

Both water permeability and salt permeability decrease with increasing feed concentration, while the mass transfer coefficient remains constant (Fig. 7A and Supplementary Table S1). The average *A* and *B* of three BW30 membranes decreased by 17% and 15% when the feed concentration increased from 1 g/L to 30 g/L, respectively. Similarly, the average *A* and *B* of three SW30 RO membranes decreased by 14% and 17% when the feed concentration increased from 1 g/L to 30 g/L, respectively. As expected, the mass transfer coefficient appears to be independent of the feed salinity and was comparable between the two types of RO membranes under the same crossflow velocity.
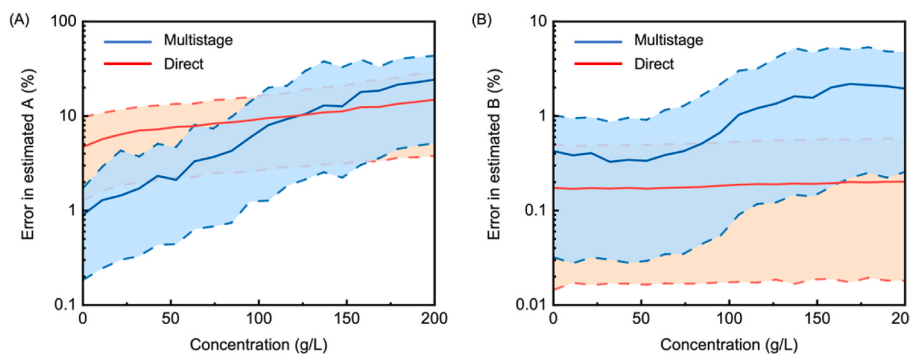
Theoretical and experimental evidence suggests that the *A* and *B* parameters of polymeric membranes are dependent on salinity. Free volume theory states that *A* and *B* decrease with a decrease in the water uptake by the membrane [21]. As previously described, increasing the external salt concentration induces the osmotic de-swelling of the membranes and decreases the thermodynamic activity of water in the solution.

While previous studies led to an inconclusive understanding of trends in *A* and *B* with increasing salinity [21,43,44], the results of our measurement provide direct evidence of the theoretical dependence of *A* and *B* on feed concentration. Two prior studies used the direct RO and FO characterization method to measure the effect of salinity on membrane transport parameters but concluded that *A* and *B* parameters either increased, decreased, or remained unchanged with increasing salinity. This incomplete observation is highly likely to be caused by the uncertainty of the direct characterization method and its low tolerance to inevitable experimental errors. In contrast, our proposed method uses a multi-stage strategy and a data-driven experimental protocol to minimize the effect of methodological errors, random errors, and biased errors on the estimates of *A* and *B*. Therefore, we successfully captured the decreasing trends of both *A* and *B* with increasing salinity as is consistent with transport theory.

Validation of the mass transfer coefficient using an empirical method matches the estimated *k* using our proposed method at near dilute conditions but shows slight deviations with increasing salinity. The difference in *k* determined using the empirical method and our proposed method is as low as 4% in the RO experiments with BW30 membranes, and 16% in the RO experiments with SW30 membranes, in 1 g/L feed solution. The difference increases up to 50% when the feed concentration is above 10 g/L, however, which was close to the level of deviation reported in the original study. Sutzkover et al. found the deviation in measured *k* and literature values increases from 3% to 102% when the Reynolds number increases from 2629 to 19344 [30]. We hypothesize that the uncertainty stems from the low tolerance of experimental errors using a single-stage measurement method, similar to the direct RO membrane characterization method. Nevertheless, the magnitude of *k* determined using our proposed method and the empirical method remains at the same level.

3.3.2. Effect of crossflow velocity on k

Mass transfer coefficient increases with increasing crossflow velocity, while *A* and *B* remain nearly constant (Fig. 7B and Supplementary Table S1) The average *k* in the boundary layer of three BW30 RO membranes and three SW30 RO membranes increased by 7% and 13%, respectively, when the crossflow velocity increased from 5.57 cm/s to 11.2 cm/s. Note that the difference of measured *k* parameters between

Fig. 8. Accuracy of multi-stage RO method and direct RO characterization method. A random error (up to ± 0.5%) was added to all process parameters including feed and permeate concentration, water and salt flux, pressure, temperature, and flow rate. A biased error (up to + 5%) was added to pressure. The blue solid line represents the median error of *A* and *B* estimated using the multi-stage RO method, and the red solid line represents the median error of A and B estimated using the direct RO method. The blue dashed line represents the 95th percentile error of *A* and *B* estimated using the multi-stage RO method, and the red dashed line represents the 95th percentile error of *A* and *B* estimated using the direct RO method. We do not recommend using the multistage method above 100 g/L TDS. (For interpretation of the references to color in this figure legend, the reader is referred to the Web version of this article.)

two types of membranes decreases with the increasing crossflow velocity because our RO system becomes more stable at higher velocity. Nevertheless, the magnitude of *k* parameters at 5.57 cm/s is similar across the six RO membranes tested in this study. In addition, the difference between the measure *k* using the empirical method and our proposed method is 4% and 16% in the RO experiments with BW30 and SW30 at the crossflow velocity of 11.2 cm/s. The deviation in *k* increases to 11% and 24% when the crossflow velocity decreases to 5.57 cm/s because our RO system is less stable at low crossflow velocity, as well as the imprecision in experimentally measured water flux.

3.4. Persistent challenges in determining A and B at high salinities

Extending the operational range of membrane-based desalination systems is critical for several emerging processes, including high-pressure reverse osmosis (HPRO) and osmotically assisted reverse osmosis (OARO), for high-salinity brine treatment [45]. The optimal design of these processes requires accurate estimates of membrane transport properties across the full salinity range [46]. Our prior analysis compared the existing empirical methods in characterizing membrane parameters in RO/HPRO, FO, PRO, and OARO, and identified the inadequacy of these methods to quantify the effect of salinity on water permeability and salt permeability [21].

We performed an accuracy analysis of our proposed method and the direct RO method in high-salinity conditions (Fig. 8). The multi-stage method continues to achieve a more accurate determination of A and B parameters by averaging out the random measurement errors up to 100 g/L. However, we also find that the errors in *A* and *B* estimated from the multi-stage method increase exponentially with salinity and exceed the errors in *A* and *B* estimated from the direct RO method above 100 g/L. This uncertainty in the actual *A* and *B* values makes it challenging to resolve the effects of high feedwater salinity on membrane transport properties and assure the membrane performance in high salinity process applications. We further note that the direct method requires an accurate estimate of mass transport coefficients, which might be difficult to acquire for high salinity conditions, preventing application of the direct method.

4. Conclusion

A simple protocol for simultaneously determining the transport properties of RO membranes and the mass transfer coefficient in the boundary layer is developed based on a data-driven design to maximize accuracy. A single RO experiment is divided into five stages, each using a different applied pressure while maintaining a constant feed concentration. We developed an algorithm to fit a group of five experiment conditions to the RO mass transport model using *A*, *B*, and *k* as regression parameters. *A, B*, and *k* are determined by minimizing the global

error in the estimated fluxes and measured values. We performed a systematic accuracy analysis to validate the robustness of the proposed method compared to the direct calculation method. Furthermore, this analysis aids the development of a data-driven protocol of RO experiment to minimize the effect of measurement errors on the estimated parameters. Following this protocol, we characterized two types of commercial TFC-PA RO membranes. The results of our measurement demonstrated that both *A* and *B* decreased with increasing salinity, and *k* increased with increasing crossflow velocity. While the proposed method enables high-precision characterization of *A* and *B* at low-salinity conditions by minimizing the effect of random errors, the determination of *A* and *B* at high-salinity conditions remains inaccurate using this method. The development of direct or higher accuracy empirical methods is an important step to fully quantifying the effect of high salinity on membrane transport properties.

CRediT authorship contribution statement

Yuanzhe Liang: Conceptualization, Methodology, Investigation, Data curation, Data collection, Formal analysis, Writing – original draft, review & editing. **Alexander V. Dudchenko**: Conceptualization, Writing – review & editing. **Meagan S. Mauter**: Conceptualization, Writing – review & editing, Project administration, Funding acquisition.

Declaration of competing interest

The authors declare that they have no known competing financial interests or personal relationships that could have appeared to influence the work reported in this paper.

Data availability

Data will be made available on request.

Appendix A. Supplementary data

Supplementary data to this article can be found online at https://doi.org/10.1016/j.memsci.2023.121686.

References

[1] M. Elimelech, W.A. Phillip, The future of seawater desalination: energy, technology, and the environment, Science 80 (333) (2011) 712–717, https://doi.org/10.1126/science.1200488.

[2] K.P. Lee, T.C. Arnot, D. Mattia, A review of reverse osmosis membrane materials for desalination-Development to date and future potential, J. Membr. Sci. 370 (2011) 1–22, https://doi.org/10.1016/j.memsci.2010.12.036.

[3] R.J. Petersen, Composite reverse osmosis and nanofiltration membranes, J. Membr. Sci. 83 (1993) 81–150, https://doi.org/10.1016/0376-7388(93)80014-O.

[4] P.W. Bohn, M. Elimelech, J.G. Georgiadis, B.J. Mariñas, A.M. Mayes, A.M. Mayes, Science and technology for water purification in the coming decades, in: Nanosci. Technol. A Collect. Rev. From Nat. Journals, World Scientific, 2009, pp. 337–346, https://doi.org/10.1142/9789814287005_0035.

[5] Y. Liang, Y. Zhu, C. Liu, K.R. Lee, W.S. Hung, Z. Wang, Y. Li, M. Elimelech, J. Jin, S. Lin, Polyamide nanofiltration membrane with highly uniform sub-nanometre pores for sub-1 Å precision separation, Nat. Commun. 11 (2020) 1–9, https://doi.org/10.1038/s41467-020-15771-2.

[6] J.R. Werber, C.O. Osuji, M. Elimelech, Materials for next-generation desalination and water purification membranes, Nat. Rev. Mater. 1 (2016), https://doi.org/10.1038/natrevmats.2016.18.

[7] Y. Liang, S. Lin, Intercalation of zwitterionic surfactants dramatically enhances the performance of low-pressure nanofiltration membrane, J. Membr. Sci. 596 (2020), 117726, https://doi.org/10.1016/j.memsci.2019.117726.

[8] L.F. Greenlee, D.F. Lawler, B.D. Freeman, B. Marrot, P. Moulin, Reverse osmosis desalination: water sources, technology, and today's challenges, Water Res. 43 (2009) 2317–2348.

[9] A.D. Khawaji, I.K. Kutubkhanah, J.-M. Wie, Advances in seawater desalination technologies, Desalination 221 (2008) 47–69.

[10] D.M. Davenport, C.L. Ritt, R. Verbeke, M. Dickmann, W. Egger, I.F.J. Vankelecom, M. Elimelech, Thin film composite membrane compaction in high-pressure reverse osmosis, J. Membr. Sci. 610 (2020), https://doi.org/10.1016/j.memsci.2020.118268.

[11] T. Tong, M. Elimelech, The global rise of zero liquid discharge for wastewater management: drivers, technologies, and future directions, Environ. Sci. Technol. 50 (2016) 6846–6855, https://doi.org/10.1021/acs.est.6b01000.

[12] A. V Dudchenko, T. V Bartholomew, M.S. Mauter, High-impact innovations for high-salinity membrane desalination, Proc. Natl. Acad. Sci. USA 118 (2021).

[13] A.G. Fane, R. Wang, M.X. Hu, Synthetic membranes for water purification: status and future, Angew. Chem. Int. Ed. 54 (2015) 3368–3386, https://doi.org/10.1002/anie.201409783.

[14] Y. Liang, S. Lin, Mechanism of permselectivity enhancement in polyelectrolyte-dense nanofiltration membranes via surfactant-assembly intercalation, Environ. Sci. Technol. 55 (1) (2020) 738–748.

[15] X. Teng, W. Fang, Y. Liang, S. Lin, H. Lin, S. Liu, Z. Wang, Y. Zhu, J. Jin, High-performance polyamide nanofiltration membrane with arch-bridge structure on a highly hydrated cellulose nanofiber support, Sci. China Mater. (2020), https://doi.org/10.1007/s40843-020-1335-x.

[16] P.M. Biesheuvel, S. Porada, M. Elimelech, J.E. Dykstra, Tutorial review of reverse osmosis and electrodialysis, J. Membr. Sci. (2022), 120221.

[17] S. Kim, E.M.V. Hoek, Modeling concentration polarization in reverse osmosis processes, Desalination 186 (2005) 111–128, https://doi.org/10.1016/j.desal.2005.05.017.

[18] V. Gekas, B. Hallström, Mass transfer in the membrane concentration polarization layer under turbulent cross flow: I. Critical literature review and adaptation of existing sherwood correlations to membrane operations, J. Membr. Sci. 30 (1987) 153–170.

[19] D.R. Paul, Reformulation of the solution-diffusion theory of reverse osmosis, J. Membr. Sci. 241 (2004) 371–386, https://doi.org/10.1016/j.memsci.2004.05.026.

[20] R.W. Baker, Membrane Technology and Applications, John Wiley & Sons, 2012, https://doi.org/10.1002/9781118359686.

[21] Y. Liang, A. V Dudchenko, M.S. Mauter, Inadequacy of current approaches for characterizing membrane transport properties at high salinities, J. Membr. Sci. (2022), 121246.

[22] A. Tiraferri, N.Y. Yip, A.P. Straub, S. Romero-Vargas Castrillon, M. Elimelech, A method for the simultaneous determination of transport and structural parameters of forward osmosis membranes, J. Membr. Sci. 444 (2013) 523–538, https://doi.org/10.1016/j.memsci.2013.05.023.

[23] M.A. Ebrahim, S. Karan, A.G. Livingston, On the influence of salt concentration on the transport properties of reverse osmosis membranes in high pressure and high recovery desalination, J. Membr. Sci. 594 (2020), 117339.

[24] N.Y. Yip, A. Tiraferri, W.A. Phillip, J.D. Schiffman, L.A. Hoover, Y.C. Kim, M. Elimelech, Thin-film composite pressure retarded osmosis membranes for sustainable power generation from salinity gradients, Environ. Sci. Technol. 45 (2011) 4360–4369.

[25] A.V. Dudchenko, M. Hardikar, A. Anand, R. Xin, R. Wang, C. Gopu, M.S. Mauter, Guidance on nusselt number correlation selection in membrane distillation, ACS ES&T Eng. 2 (8) (2022) 1425–1434.

[26] A.L. Zydney, Stagnant film model for concentration polarization in membrane systems, J. Membr. Sci. 130 (1997) 275–281, https://doi.org/10.1016/S0376-7388(97)00006-9.

[27] L. Song, M. Elimelech, Theory of concentration polarization in crossflow filtration, J. Chem. Soc., Faraday Trans. 91 (1995) 3389–3398.

[28] L. Song, S. Yu, Concentration polarization in cross flow reverse osmosis, AIChE J. 45 (1999) 921–928.

[29] J.R. McCutcheon, R.L. McGinnis, M. Elimelech, Desalination by ammonia - carbon dioxide forward osmosis: influence of draw and feed solution concentrations on process performance, J. Membr. Sci. 278 (2006) 114–123.

[30] I. Sutzkover, D. Hasson, R. Semiat, Simple technique for measuring the concentration polarization level in a reverse osmosis system, Desalination 131 (2000) 117–127, https://doi.org/10.1016/S0011-9164(00)90012-2.

[31] J.G. Wijmans, R.W. Baker, The solut.-diff. model : Rev. 107 (1995) 1–21.

[32] P. Virtanen, R. Gommers, T.E. Oliphant, M. Haberland, T. Reddy, D. Cournapeau, E. Burovski, P. Peterson, W. Weckesser, J. Bright, SciPy 1.0: fundamental algorithms for scientific computing in Python, Nat. Methods 17 (2020) 261–272.

[33] W.R. Esposito, C.A. Floudas, Global optimization in parameter estimation of nonlinear algebraic models via the error-in-variables approach, Ind. Eng. Chem. Res. 37 (1998) 1841–1858, https://doi.org/10.1021/ie970852g.

[34] Y. Bard, Nonlinear Parameter Estimation, 1974.

[35] M.F.A. Goosen, S.S. Sablani, S.S. Al-Maskari, R.H. Al-Belushi, M. Wilf, Effect of feed temperature on permeate flux and mass transfer coefficient in spiral-wound reverse osmosis systems, Desalination 144 (2002) 367–372.

[36] M. Aghajani, M. Wang, L.M. Cox, J.P. Killgore, A.R. Greenberg, Y. Ding, Influence of support-layer deformation on the intrinsic resistance of thin film composite membranes, J. Membr. Sci. 567 (2018) 49–57, https://doi.org/10.1016/j.memsci.2018.09.031.

[37] M.R. Chowdhury, J. Ren, K. Reimund, J.R. McCutcheon, A hybrid dead-end/cross-flow forward osmosis system for evaluating osmotic flux performance at high recovery of produced water, Desalination 421 (2017) 127–134.

[38] M.H. Sharqawy, J.H. Lienhard V, S.M. Zubair, Thermophysical properties of seawater: a review of existing correlations and data, Desalination Water Treat. 16 (2010) 354–380, https://doi.org/10.5004/dwt.2010.1079.

[39] H.I. Britt, R.H. Luecke, The estimation of parameters in nonlinear, implicit models, Technometrics 15 (1973) 233–247, https://doi.org/10.1080/00401706.1973.10489037.

[40] G.M. Geise, D.R. Paul, B.D. Freeman, Fundamental water and salt transport properties of polymeric materials, Prog. Polym. Sci. 39 (2014) 1–42, https://doi.org/10.1016/j.progpolymsci.2013.07.001.

[41] J.R. McCutcheon, M. Elimelech, Influence of concentrative and dilutive internal concentration polarization on flux behavior in forward osmosis, J. Membr. Sci. 284 (2006) 237–247.

[42] V.M.M. Lobo, M. Helena, S.F. Teixeira, Diffusion coefficients in aqueous solutions of hydrochloric acid at 298 K, Electrochim, Acta 24 (1979) 565–567.

[43] E.S. Jang, J. Kamcev, K. Kobayashi, N. Yan, R. Sujanani, T.J. Dilenschneider, H. B. Park, D.R. Paul, B.D. Freeman, Influence of water content on alkali metal chloride transport in cross-linked Poly(ethylene glycol) diacrylate.2. Ion diffusion, Polymer (Guildf) 192 (2020), 122316, https://doi.org/10.1016/j.polymer.2020.122316.

[44] G.M. Geise, C.M. Doherty, A.J. Hill, B.D. Freeman, D.R. Paul, Free volume characterization of sulfonated styrenic pentablock copolymers using positron annihilation lifetime spectroscopy, J. Membr. Sci. 453 (2014) 425–434.

[45] T.V. Bartholomew, L. Mey, J.T. Arena, N.S. Siefert, M.S. Mauter, Osmotically assisted reverse osmosis for high salinity brine treatment, Desalination 421 (2017) 3–11, https://doi.org/10.1016/j.desal.2017.04.012.

[46] T.V. Bartholomew, N.S. Siefert, M.S. Mauter, Cost optimization of osmotically assisted reverse osmosis, Environ. Sci. Technol. 52 (2018) 11813–11821, https://doi.org/10.1021/acs.est.8b02771.